nature portfolio

https://doi.org/10.1038/s41567-021-01400-2

Supplementary information

Spectrally periodic pulses for enhancement of optical nonlinear effects

In the format provided by the authors and unedited

Supplementary Information - Spectrally periodic pulses for enhancement of optical nonlinear effects

Joshua P. Lourdesamy[1], Antoine F. J. Runge[1,*], Tristram J. Alexander[1], Darren D. Hudson[2], Andrea Blanco-Redondo[3], and C. Martijn de Sterke[1,4]

[1]Institute of Photonics and Optical Sciences (IPOS), The University of Sydney, NSW 2006, Australia
[2]CACI Photonics Solutions, 15 Vreeland Road, Florham Park, NJ 07932, USA.
[2]Nokia Bell Labs, 791 Holmdel Road, Holmdel, NJ 07733, USA.
[4]The University of Sydney Nano Institute (Sydney Nano), The University of Sydney, NSW 2006, Australia.
[*]Corresponding author Email: antoine.runge@sydney.edu.au

ABSTRACT

This article contains supplementary information to the manuscript entitled “Spectrally periodic pulses for enhancement of optical nonlinear effects. It presents a schematic of the experimental setup as well as supplementary information about the experimental mode-locking parameters. In addition, we provide full details of the multiple scale analysis used to derive the expression for the nonlinear enhancement factor.

1 Fiber laser

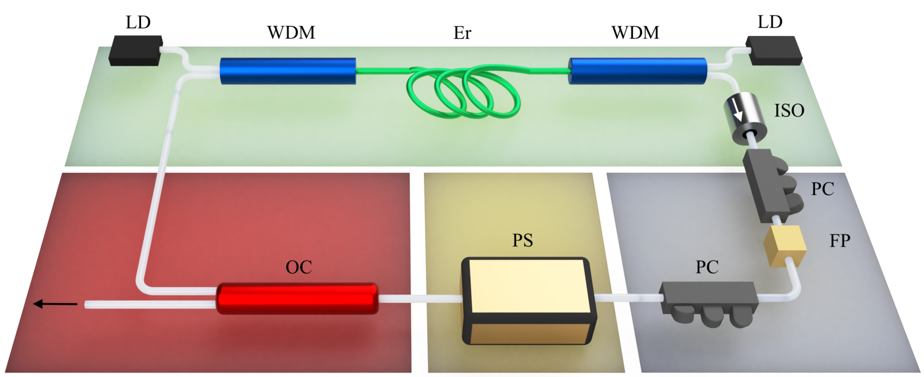

Figure 1. Laser cavity for generation of spectrally periodic pulses. LD, laser diode; ISO, optical isolator; PC, polarization controller; FP, in-line fibre polarizer; PS, pulse shaper; OC, output coupler; WDM, wavelength division multiplexers; Er, erbium-doped fibre.

A schematic of the laser cavity is shown in Fig. 1. It is an erbium-doped fibre laser that uses nonlinear polarization evolution for mode-locking and incorporates an intracavity programmable optical pulse shaper.[1,2] The total cavity length $L = 18.2$ m. Two laser diodes producing light at 980 nm were used to couple light into the cavity through two 980/1550 nm wavelength division multiplexers. An optical isolator ensures that light can only propagate in one direction within the cavity. Passive mode-locking is achieved using two fibre polarisation controllers and a fibre polariser to serve as an artificial saturable absorber. At a pump power of approximately 500 mW, the laser is self-starting and multi-pulsing after adjusting the polarisation controller. Single pulsing is achieved by reducing the pump power to approximately 180 mW. The laser incorporates a programmable spectral pulse-shaper (WaveShaper) which is used to tailor the net-cavity dispersion by applying a phase mask of the form

$$\phi(\omega) = L\left(\left(\frac{\beta_{2,\mathrm{smf}}(\omega-\omega_0)^2}{2} + \frac{\beta_{3,\mathrm{smf}}(\omega-\omega_0)^3}{6}\right) + \sum_{n=2,4,\cdots}^{N} (-1)^{\frac{n}{2}} \frac{\beta_n}{n!}(\omega-\omega_0)^n\right). \tag{1}$$

The first and second terms on the right-hand side correspond to the applied phase that compensates the quadratic and cubic dispersion of the rest of the cavity, respectively, which is dominated by single-mode fibre (SMF) segments. The cavity length is

$L = 18.2$ m, and $\beta_{2,\mathrm{smf}} = +21.4$ ps^2 km^{-1} and $\beta_{3,\mathrm{smf}} = -0.12$ ps^3 km^{-1} based on values reported earlier for similar SMF.[1,3] The third term in Eq. (1) represents the combination of even-order contributions that generate the required dispersion.

2 Laser dynamics simulations

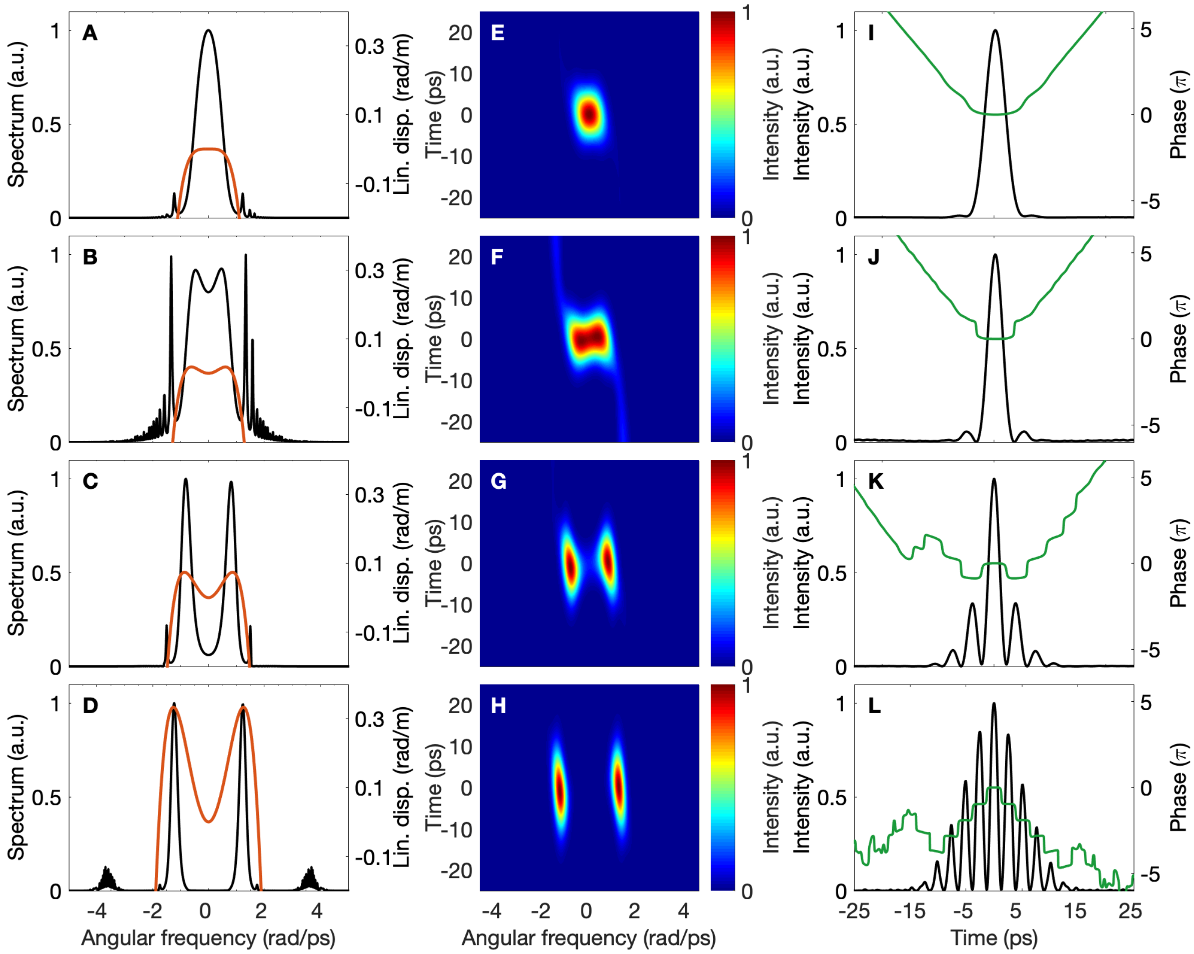

Figure 2. Numerical simulations of laser output with parameter values matching experimental values from Fig. 2. Moving from row 1 to 4, $\beta_2 = 0,\ 200,\ 400$ and 850 ps^2 km^{-1}. The net cubic and quartic dispersion are fixed at $\beta_3 = 0$ ps^3 km^{-1} and $\beta_4 = -3250$ ps^4 km^{-1}. (**A-D**) Simulated output spectra (black) and linear dispersion relation (Lin. disp.) (orange). (**E-H**) Simulated spectrograms. (**I-L**) Simulated temporal intensity profiles (black) and temporal phase (green).

We model the cavity dynamics using an iterative cavity map.[1,4,5] The propagation through each element is calculated by solving the NLSE with Kerr nonlinearity and appropriate dispersion.[1] The full set of simulated output pulse characteristics for the experimental cases presented in Fig. 2 (see main text) are shown in Fig. 2. The first column shows the pulse spectra. In all cases the simulated pulses (black curves) are in very good agreement with the experimental results. The second column shows the simulated spectrograms, these are in good agreement with those shown in Fig. 2. The final column shows the temporal profiles of the pulses. The experimental and the simulated (black curves) intensities are in excellent agreement, with both the positions and amplitudes of the fringes matching well in all cases. The simulated (green) phase also agrees well, with the differences attributed to arbitrary differences in direction of the π phase flips that correspond to the intensity nodes.

3 Comparison between conventional soliton and $J = 2$ counterpart.

We directly compare a measured $J = 2$ spectrally periodic soliton to its corresponding conventional soliton counterpart, by operating the laser in the regime corresponding to the fourth row of Fig. 2 in the main text. We then apply losses at the high-frequency component around 1.26 rad/ps using the pulse-shaper. The measured output spectrum is shown in Fig. 3A (blue curve) and shows a single, conventional soliton centred around -1.26 rad/ps. This is consistent with the corresponding spectrogram shown in the inset. The white dashed lines indicate the locations of the peaks and the central frequency of the linear dispersion. The retrieved normalized temporal intensity profile is shown in Fig. 3B (blue curve). The temporal fringes have vanished, and the pulse exhibits a conventional soliton shape, which corresponds to the envelope function of the $J = 2$ spectrally periodic soliton from Fig. 2L (black dashed curve) in the main text. The retrieved phase in Fig. 3B (yellow curve) is linear across the entire pulse width. This linear phase arises from the offset between the single soliton and the reference frequency ω_0. Its slope can be understood by the following argument. The offset of 1.61 nm corresponds to a difference in angular frequency of 1.26 rad ps^{-1}, which, for the 9.49 ps retrieved pulse width corresponds to a phase of 3.78π, in excellent agreement with the measured value of 3.81π.

From these experiments we also measure the energy of each pulse. As both measured $J = 1$ and 2 solitons have the same local quadratic dispersion $\bar{\beta}_2$ and pulse widths, we can directly compare their respective energy and calculate the nonlinear enhancement factor $\mathscr{E}_2 = E_1/E_2 = 365.4$ pJ$/251.1$ pJ $= 1.46$. This is in excellent agreement with the predicted value of $3/2$ (see Section 3B in the main text). Thus a soliton with $J = 2$ spectral components requires two-thirds of the energy of its conventional counterpart. The measured peak powers for $J = 1$ and 2 were 3.71 W and 5.08 W, respectively. This corresponds to a ratio of 0.73, again in excellent agreement with the predicted value of 0.75. These results are strong evidence of the enhancement of the nonlinear effect through dispersion engineering and demonstrate the unprecedented level of dispersion control allowed by our experimental setup.

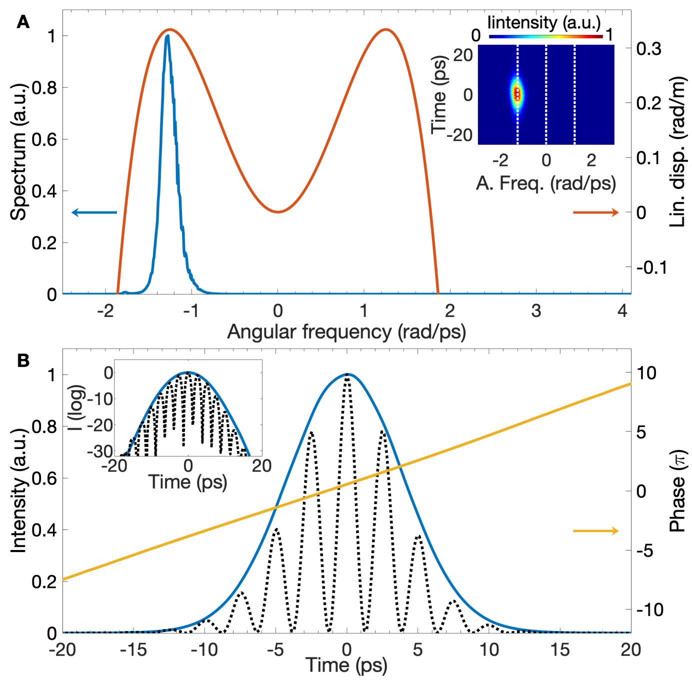

Figure 3. Comparison of *J*=1 and 2. (**A**) Measured output spectrum for $J = 1$ soliton (blue curve) obtained by applying a loss at 1.26 rad/ps. Linear dispersion relation (orange curve). Inset: measured spectrogram with white dashed lines denoting the locations of the peaks and central frequency in the dispersion relation. (**B**) Retrieved temporal intensity (blue curve) and temporal phase (yellow curve) for $J = 1$ and retrieved temporal intensity for $J = 2$ (dashed black curve). Inset: temporal intensities on log scale.

4 Dispersion relations for $J = 3,\ 4,\ 5$

For $J = 3,\ 4$ and 5 the functions used to define each dispersion relation was a tenth, sixteenth and eighteenth order polynomial respectively. These are defined by setting the following: the desired $\bar{\beta}_2$, the frequency ($\delta\omega$) of the lowest order maximum not centered at ω_0, $\beta_1 = \beta_3 = 0$ at each maximum, each maximum is evenly spaced and has the same height. Note that $\delta\omega = \Delta\omega$ for $J = 3,\ 5$ and $2\delta\omega = \Delta\omega$ for $J = 4$. For the numerical results presented in Fig. 1 of the main text, $\delta\omega = 6.42,\ 4.30,\ 6.42$ rad ps^{-1} for $J = 3,\ 4$ and 5 respectively. For the experimental results discussed in Sec. IIB in the main text, $\delta\omega = 1.8,\ 0.8,\ 1.5$ rad ps^{-1} $J = 3,\ 4$ and 5 respectively. All values for $\bar{\beta}_2$ are provided alongside the results. By applying these conditions the coefficients required for dispersion relations of the form

$$\beta(\omega) = D_{18}\omega^{18} + D_{16}\omega^{16} + D_{14}\omega^{14} + D_{12}\omega^{12} + D_{10}\omega^{10} + D_8\omega^8 + D_6\omega^6 + D_4\omega^4 + D_2\omega^2 \tag{2}$$

for $J = 3$, 4 and 5 are provided in columns 2, 3 and 4, respectively, of Table. 1. The coefficients are defined in terms of $D_2 = 0.5\bar{\beta}_2$ and the frequency $\delta\omega$.

Table 1. Dispersion coefficients (D_n) required for $J = 3,\ 4,\ 5$.

Coefficients	$J = 3$	$J = 4$	$J = 5$
$D_4(\delta\omega^2/D_2)$	$-100/32$	$-965657/1177182$	$-105/32$
$D_6(\delta\omega^4/D_2)$	$348/96$	$1416737/5297319$	$44429/10368$
$D_8(\delta\omega^6/D_2)$	$-60/32$	$-971221/21189276$	$-40885/13824$
$D_{10}(\delta\omega^8/D_2)$	$12/32$	$24689/5297319$	$67921/55296$
$D_{12}(\delta\omega^{10}/D_2)$	-	$-3073/10594638$	$-13405/41472$
$D_{14}(\delta\omega^{12}/D_2)$	-	$55/5297319$	$1475/27648$
$D_{16}(\delta\omega^{14}/D_2)$	-	$-7/42378552$	$-35/6912$
$D_{18}(\delta\omega^{16}/D_2)$	-	-	$35/165888$

5 Multiple scales analysis

As discussed in Section III A of the main text, we search for solutions to Eq. (3), of the form given in Eq. (4). In the treatment below we take the number of frequency components J to be odd, though the argument for even J is very similar. We now rewrite Eq. (4) as

$$\varphi(\tau,z) = \frac{\varepsilon}{\mathscr{N}} f(\varepsilon\tau,\varepsilon^2 z) \sum_{j=-(J-1)/2}^{j=+(J-1)/2} p_j e^{-ij\Delta\omega\tau} \equiv \frac{\varepsilon}{\mathscr{N}} f(\varepsilon\tau,\varepsilon^2 z)\, c(\tau), \tag{3}$$

where we explicitly introduced the normalisation factor $\mathscr{N}$ and included the summation limits. The carrier can be taken to be real and symmetric and so $p_{-j} = p_j$. We then substitute the ansatz (3) into Eq. (3) and collect terms of equal order in ε. Starting at order ε^1 we find that the only contributions come from taking the time-derivatives of the carrier, leading to

$$\frac{f}{\mathscr{N}} \sum_j p_j \left(\frac{\beta_2}{2!}(j\Delta\omega)^2 + \frac{\beta_4}{4!}(j\Delta\omega)^4 + \cdots \right) e^{-ij\Delta\omega\tau} = 0. \tag{4}$$

Since our dispersion relation has the property that $\beta = 0$ at all frequencies $-(J-1)\Delta\omega/2, \ldots, (J-1)\Delta\omega/2$ (see Figs 1A-E), the term in brackets vanishes for each j and thus ansatz (4) satisfies Eq (3) to first order in ε.

At order ε^2 we find that the resulting expression contains one time derivative of f, with all the remaining time derivatives coming from the carrier

$$\frac{f_\tau}{\mathscr{N}} \sum_j p_j \left(\beta_2(j\Delta\omega) + \frac{\beta_4}{3!}(j\Delta\omega)^3 + \cdots \right) e^{-ij\Delta\omega\tau} = 0, \tag{5}$$

where f_τ indicates $\partial f/\partial\tau$. The expression in brackets corresponds to the $d\beta/d\omega$ at $-(J-1)\Delta\omega/2, \ldots, (J-1)\Delta\omega/2$. Thus, to this order the equation is satisfied, since, by assumption, the dispersion relation has a vanishing derivative at each of these frequencies (see Figs 1A-E).

At order ε^3 we obtain nontrivial results because of contributions from the z-derivative of f and from the nonlinear term. We find

$$\frac{i}{\mathscr{N}} f_z \sum_j p_j e^{-ij\Delta\omega\tau} - \frac{f_{\tau\tau}}{2\mathscr{N}} \sum_j p_j \left(\beta_2 + \frac{\beta_4}{2}(j\Delta\omega)^2 + \cdots \right) e^{-ij\Delta\omega\tau} + \frac{\gamma}{\mathscr{N}^3} |f|^2 f \sum_j \sum_{j'} \sum_{j''} p_j p_{j'} p_{j''} e^{-i(j-j'+j'')\Delta\omega\tau} = 0, \tag{6}$$

where $f_z \equiv \partial f/\partial z$. The factor in brackets in the second term represents the second derivative of the dispersion relation at each of the frequencies $j\Delta\omega$. For our assumed dispersion relation all of these equal $\bar{\beta}_2$, and so this term can be written as

$$-\frac{\bar{\beta}_2}{2} \frac{f_{\tau\tau}}{\mathscr{N}} \sum_j p_j e^{-ij\Delta\omega\tau}. \tag{7}$$

In the nonlinear term in Eq. (6) the triple sum can be written as $\sum_j q_j e^{-ij\Delta\omega\tau}$ with summation limits $\pm 3(J-1)/2$, and where the q_j are sums of triple products of the p_j. Our aim is to find a single governing equation for the envelope f. For consistency we therefore require the ratios q_j/p_j to be same for all $|j| \leq (J-1)/2$. This consistency condition is satisfied only for certain ratios of the p_j, and this argument thus fixes their relative values. Note that the q_j for $(J-1)/2 < |j| \leq 3(J-1)/2$ are associated with four-wave mixing (FWM) contributions to frequencies outside the carrier and we neglect these. Although we observe these four-wave mixing products in our experiments (see, e.g., Fig. 2D in main text) and in our simulations (see, e.g., Fig. 2M in main text), they are poorly phase matched and do not reach high intensities

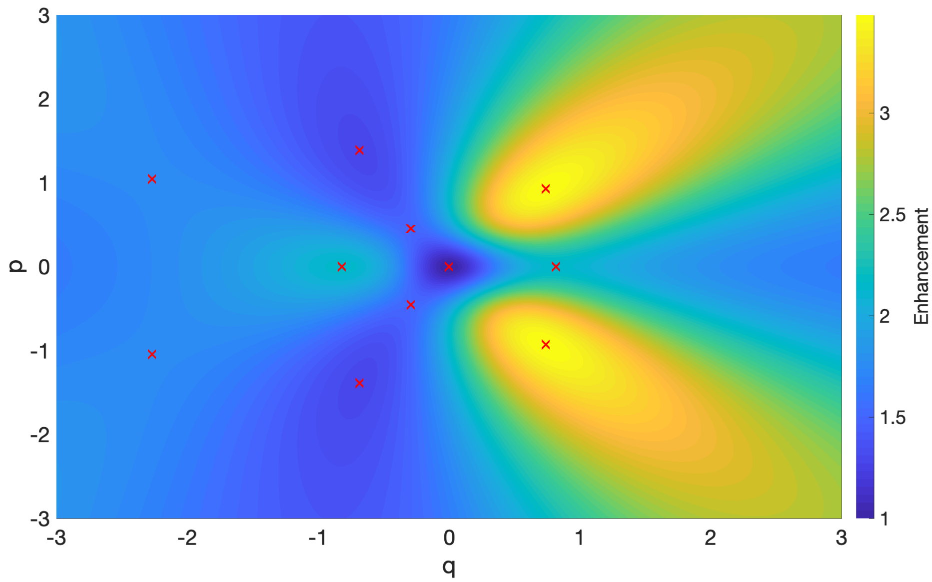

Figure 4. Theoretical nonlinear enhancement factor for $J = 5$ changing with amplitudes of frequency components. The colour-bar denotes the enhancement value and the red crosses mark the stationary points of the nonlinear enhancement with respect to the amplitudes of the frequency components.

Figure 4 describes the surface of all possible nonlinear enhancement factors for $J = 5$ as the relative amplitudes of the $p_{\pm 1}$ and $p_{\pm 2}$ frequency components are varied between -3 and 3. The red crosses mark the stationary points and these are the values for p_j which are satisfy the consistency condition. The measured pulse corresponds to the global maximum where $p_{\pm 1} = 0.930$ and $p_{\pm 2} = 0.742$.

Having established a procedure to find the amplitudes p_j, we are now in the position to find the evolution equation for the envelope f. To do so we multiply each term in Eq. (6) by $c(\tau)$ and integrate so as to average over a period $2\pi/\Delta\omega$. We then find, using Eq. (7), that f satisfies the nonlinear Schrödinger equation

$$if_z \sum_j p_j^2 - \frac{\bar{\beta}_2}{2} \sum_j p_j^2 + \gamma |f|^2 f \frac{1}{\mathcal{N}^2} \sum_j p_j q_{-j} = 0, \tag{8}$$

where the summations extend between $\pm(J-1)/2$. We now fix the normalisation such that

$$\mathcal{N} = \sum_j p_j^2, \tag{9}$$

so the carrier has unit average intensity. The effective nonlinear coefficient is then given by Eq. (6), that enters the final Eq. (5).

6 Nonlinear enhancement

Table 2 shows the nonlinear enhancement for $J = 1$ to 5. Columns 1 and 2 show the predicted and numerical values, also shown in Fig. 4 in main text. Column 3 shows the measured nonlinear enhancement factors for pulses which correspond to the $\bar{\beta}_2$ values shown in Column 4. These $\mathscr{E}_J$ were obtained by comparing the energy of each measured pulse to the expected energy of its corresponding $J = 1$ soliton, with the same pulse-width and $\bar{\beta}_2$, based on the energy-width scaling for conventional solitons.

Table 2. Nonlinear enhancement factor $\mathscr{E}_J$ for J=1 to 5. Column 1: theoretically predicted. Column 2: $\mathscr{E}_J$ determined by evaluating E_1/E_J for numerically calculated pulses. Column 3: Experimentally obtained values for $\mathscr{E}_J$ using the energy-width scaling method for the measurements in the main body corresponding to the $\bar{\beta}_2$ values in Column 4.

J	Theory $\mathscr{E}_J$	Numerics $\mathscr{E}_J$	Energy scaling $\mathscr{E}_J$	$\bar{\beta}_2$ ps^2 km^{-1}
1	1	1	0.997	-1700
2	1.5	1.51	1.46	-1700
3	2.14	2.16	2.17	-800
4	2.81	2.83	2.71	-600
5	3.48	3.49	3.85	-600

7 Radio frequency measurements

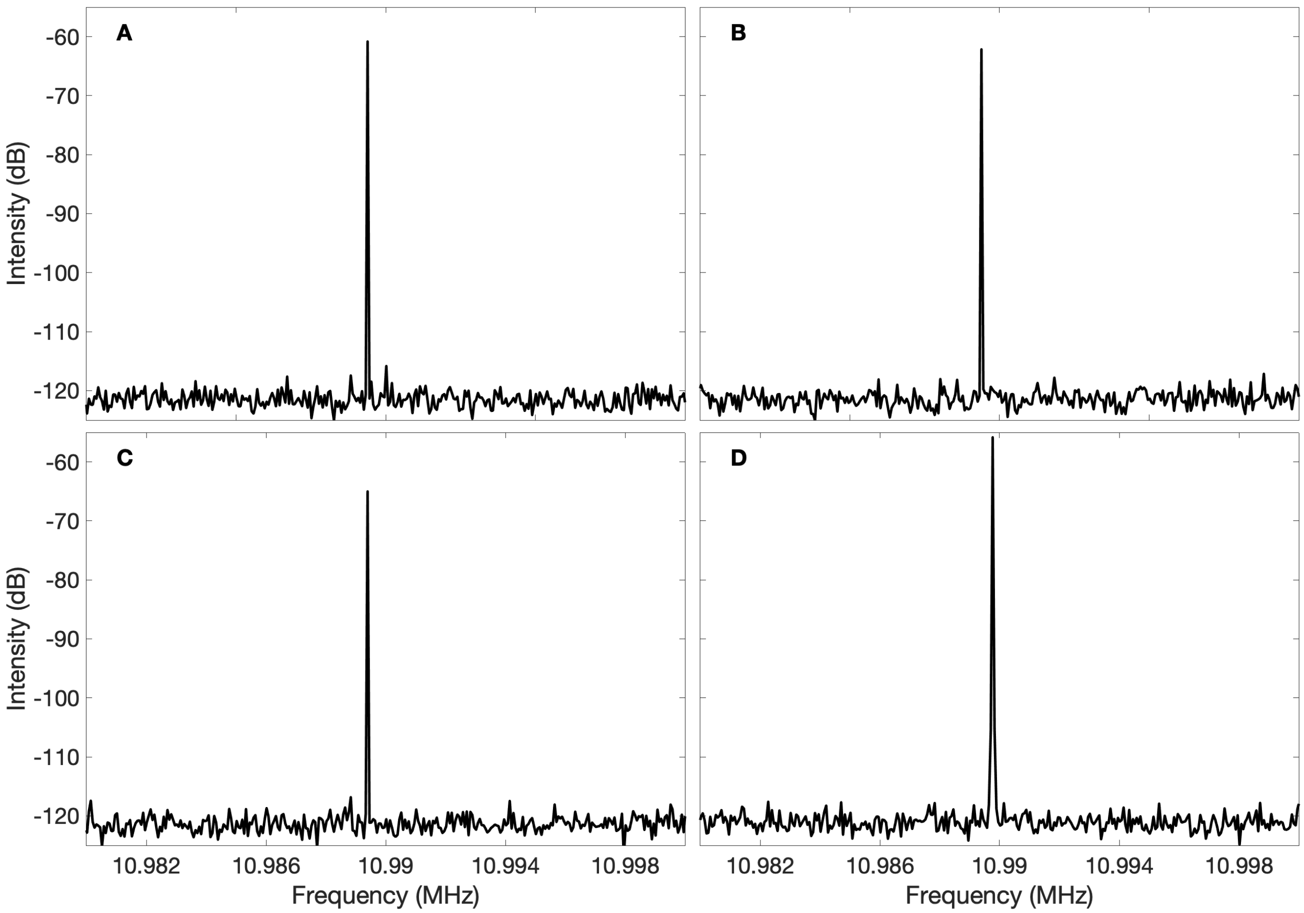

Figure 5. Radio-frequency spectra of cavity output pulse train for $J=2$. Repetition rate of cavity where quadratic dispersion is varied and cubic and quartic dispersion are fixed at $\beta_3 = 0$ ps^3 km^{-1} and $\beta_4 = -3250$ ps^4 km^{-1} respectively. **(A)** $\beta_2 = 0$ ps^2 km^{-1}. **(B)** $\beta_2 = 200$ ps^2 km^{-1}. **(C)** $\beta_2 = 400$ ps^2 km^{-1}. **(D)** $\beta_2 = 850$ ps^2 km^{-1}.

Figure 5 shows the measured RF spectra of the output pulse train for fixed for fixed β_3 and β_4 while varying β_2. Figure 5A-D correspond to $\beta_2 = 0$, 200, 400 and 850 ps^2 km^{-1} respectively. These correspond to the measurements shown in Fig. 2. Each was measured across a bandwidth of 20 MHz with a resolution of 62.5 Hz. In each case the measured RF spectrum displays a single peak, indicating that the spectral components are synchronous.

8 Propagation of $J=5$ pulse

Figure 6 shows the simulated propagation of a $J=5$ pulse over 15 dispersion lengths, corresponding to 12.3 m, through an ideal waveguide. The dispersion lengths is defined as $L_{GVD} = (T_{FWHM}/1.763)/|\bar{\beta}_2|^2$, where T_{FWHM} is the full width at half maximum of the hyperbolic secant shaped envelope of the temporal intensity profile. The linear dispersion, as defined in Eq. 2 and Table 1, is specified by $\bar{\beta}_2 = -12$ ps^2 km^{-1} and $\delta\omega = 8$ rad/ps. The input pulse is obtained by using the Newton conjugate gradient method[6] to find a stationary solution to the NLSE generalised to include the relevant orders of dispersion (see Eq. (3) in the main text). The pulse evolution is then simulated using the symmetric split-step Fourier method algorithm.[7] The simulated temporal and spectral intensity profiles of the input (blue) and output (red-dashed) pulses are shown in Fig. 6A and B, respectively. Figures 6C and D show the corresponding evolution of the temporal and spectral intensity profiles, respectively. These demonstrate that the linear and nonlinear effects balance such that the pulse propagates as a stable stationary solution.

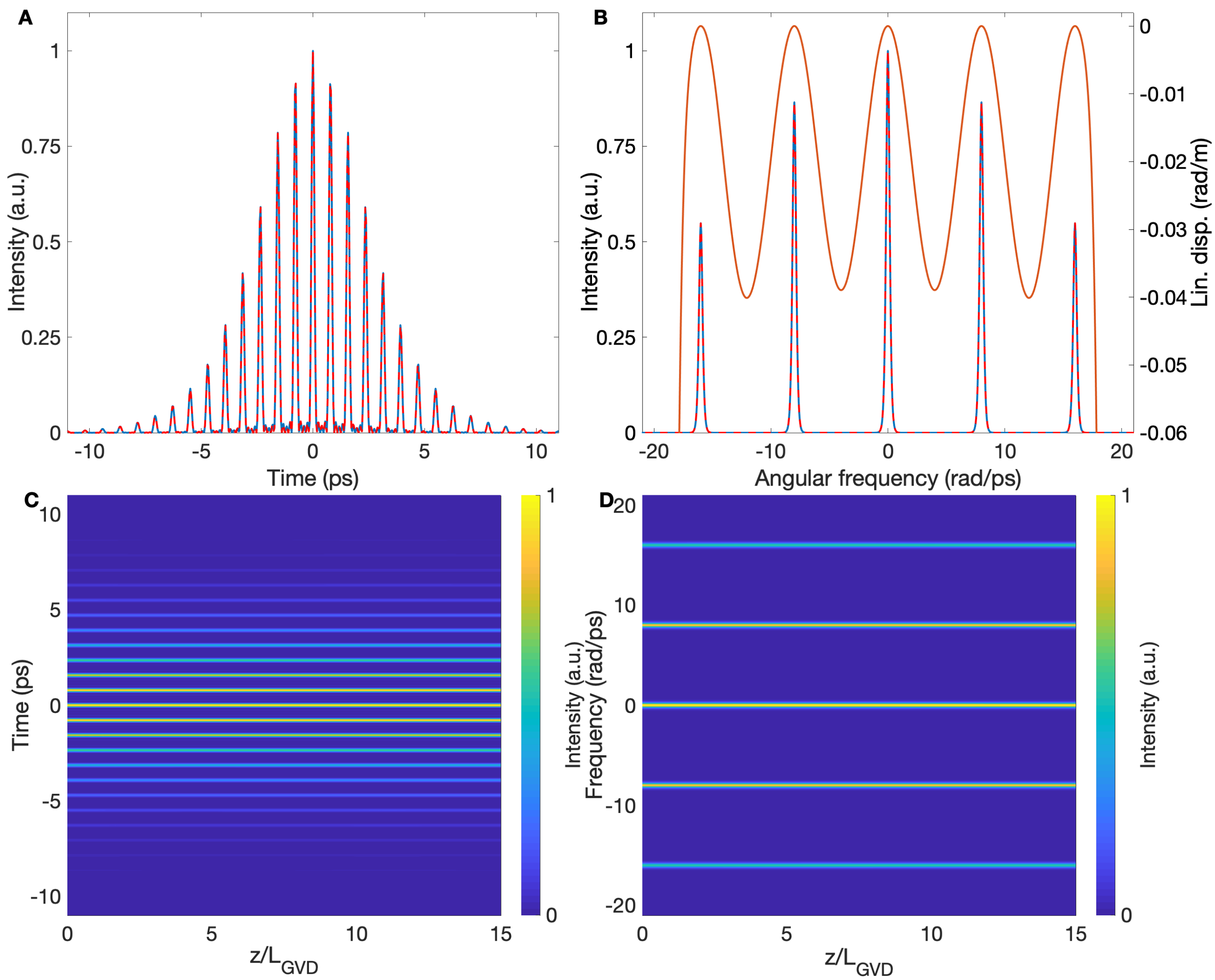

Figure 6. Evolution of $J = 5$ pulse over 15 dispersion lengths in an ideal waveguide. $\gamma = 1$ W^{-1} km^{-1}, the nonlinear phase shift $\mu = 0.6$ km^{-1} and the linear dispersion is specified by $\bar{\beta}_2 = -12$ ps^2 km^{-1} and $\delta\omega = 8$ rad ps^{-1}. **(A)** Input temporal intensity profile (blue) and output temporal intensity profile (red-dashed). **(B)** Input spectral intensity profile (blue), output spectral intensity profile (red dashed) and linear dispersion relation (Lin. disp.; orange). **(C)** Evolution of temporal intensity profile. **(D)** Evolution of spectral intensity profile.

References

1. Runge, A. F. J., Hudson, D. D., Tam, K. K. K., de Sterke, C. M. & Blanco-Redondo, A. The pure-quartic soliton laser. *Nat. Photon.* **14**, 492–497 (2020).

2. Runge, A. F. J. *et al.* Infinite hierarchy of solitons: Interaction of Kerr nonlinearity with even orders of dispersion. *Phys. Rev. Res.* **3**, 013166 (2021).

3. Hammani, K. *et al.* Peregrine soliton generation and breakup in standard telecommunications fiber. *Opt. Lett.* **36**, 112–114 (2011).

4. Oktem, B., Ülgüdür, C. & Ilday, F. Ö. Soliton-similariton fibre laser. *Nat. Photon.* **4**, 307–311 (2010).

5. Woodward, R. I. Dispersion engineering of mode-locked fibre lasers. *J. Opt.* **20**, 033002 (2018).

6. Yang, J. Newton-conjugate-gradient methods for solitary wave computations. *J. Comput. Phys.* **228**, 7007–7024 (2009).

7. Agrawal, G. D. *Nonlinear Fiber Optics* (Academic Press, 1995).